Orienting Unorganized Points for Surface Reconstruction

Shengjun Liu   Charlie C.L. Wang*
Department of Mechanical and Automation Engineering,
The Chinese University of Hong Kong, China

Abstract—**We address the problem of assigning consistently oriented normal vectors to unorganized point cloud with noises, non-uniformities, and thin-sharp features as a pre-processing step to surface reconstruction. The conventional orienting scheme using minimal spanning tree fails on points with the above defects. Different from the recently developed consolidation technique, our approach does not modify (i.e., down-sampling) the given point cloud so that we can reconstruct more surface details in the regions with very few points. The method consists of three major steps. We first propose a modified scheme of generating adaptive spherical cover for unorganized points by adding a sphere splitting step based on eigenvalue analysis. This modification can better preserve the connectivity of surface generated from the spheres in the highly sparse region. After generating the triangular mesh surface and cleaning its topology, a local search based algorithm is conducted to find the closest triangle to every input points and then specify their orientations. Lastly, an orientation-aware principle component analysis step gives correct and consistently oriented normal vectors to the unorganized input points. Conventional implicit surface fitting based approach can successfully reconstruct high quality surfaces from the unorganized point cloud with the help of consistently oriented normal vectors generated by our method.**

Keywords—**orientation; consistency; unorganized points; PCA; surface reconstruction.**

1. INTRODUCTION

The reverse engineering problem for reconstructing three dimensional models in a computer system from unorganized points that are generated by 3D surface scanning devices has been a subject of intensive research for many years. The scanned 3D surface represented by an unorganized point cloud is typically noisy, contains holes, and has high variations in point density. Oriented normals at the points play a critical role in surface reconstruction. It is because that the oriented normals define the reconstructed surface to the first order and identify the inside/outside information. As will be shown in our tests below, the oriented normals become extremely important at the regions with very sparse points. Also, to generate correctly oriented normal vectors on the points

in such regions is a very tough job. The conventional methods using *minimal spanning tree* (MST) (e.g., [1]) or Voronoi diagram (e.g., [2], [3], [4]) fail. Some recent researches consider estimating normals from captured images using photometric stereo [5], [6], which however suffers from the unideal acquisition conditions like specular reflections, material artifacts, and shadowing. The most recent work presented in [7] does not assign normal vectors directly to the given points. It first adopts a weighted locally optimal projection operator to produce a set of denoised and evenly distributed particles over the original point cloud, and then conducts a priority-driven normal propagation scheme to assign normal vectors to the particles. This down-sampling strategy actually further removes limited information of underlying surfaces from those highly sparse regions, therefore the reconstructed surface in such regions will not be as good as ours (see Fig.1). Our approach proposed in this paper can assign consistently oriented normal vectors to the scattered points so that the downstream reconstruction algorithm can successfully generate surface in the regions with highly sparse points.

To orient unorganized points effectively and efficiently, we develop two techniques by extending the integrating approach for meshing scattered point data [8]. First, a modified scheme is proposed to generate *Adaptive Spherical Cover* (ASC) for unorganized points by adding an eigenvalue analysis based sphere splitting step. With this step, our approach can better preserve the surface's connectivity in the regions with highly sparse points. After getting the spherical cover for scattered points, the triangulation and topology cleaning procedure (ref. [8]) can generate a triangular mesh surface M roughly presenting the underlying surface S. Although this mesh M is not a good approximation of S, it gives a very robust evidence for assigning the orientation of input points. A straightforward way is to find the closest point $\mathbf{c}_p$ on M for each input point $\mathbf{p}$, then the normal vector $\mathbf{n}_{\mathbf{c}_p}$ of $\mathbf{c}_p$ on M is assigned as the normal vector of $\mathbf{p}$. Nevertheless, as M is an inaccurate approximation of S, such normal vectors give inaccurate surface information to the downstream mesh reconstruction algorithm (e.g., [9]). Therefore, instead of assigning $\mathbf{n}_{\mathbf{c}_p}$ to $\mathbf{p}$, we only let $\mathbf{p}$ hold the orientation of $\mathbf{n}_{\mathbf{c}_p}$ – thus, we name our method as *orienting* approach (ORT). An orientation-aware *Principle Component Analysis* (PCA) step is adopted to assign correct and consistently oriented normal vectors to the unorganized points. Moreover, the ASC constructed in the first step will be employed to speed up the

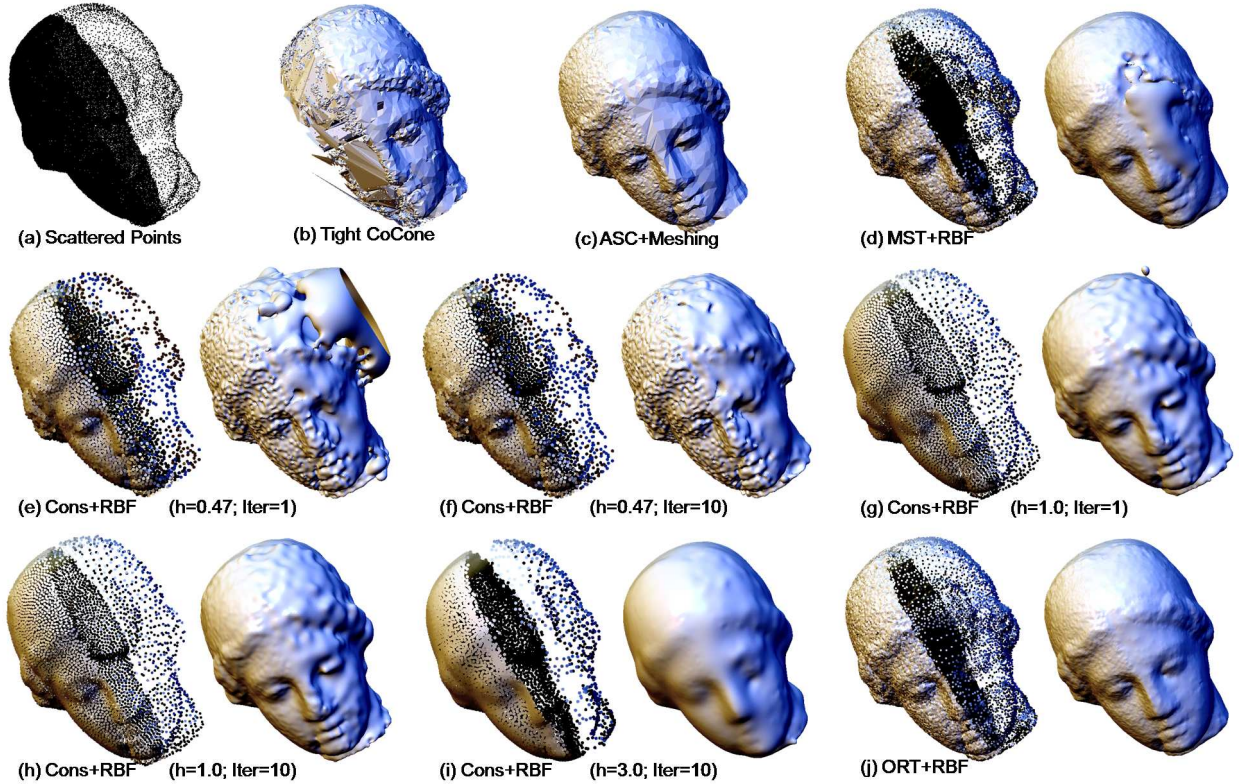*Corresponding Author. E-mail:cwang@mae.cuhk.edu.hk

Fig. 1. Surface reconstruction results on (a) the Venus model (72.5k points) with noises and non-uniform point density by different approaches, including: (b) Tight CoCone [4], (c) the integrating approach with *adaptive spherical cover* (ASC) followed by a meshing step [8], (d) the conventional *minimal spanning tree* (MST) based normal estimation [1] followed by a *radial basis function* (RBF) based surface reconstruction [9], (e)-(i) the point cloud *consolidation* (Cons) [7] followed by RBF-based surface reconstruction, and (j) our orienting approach (ORT) with RBF-based reconstruction. For those resultant mesh surfaces generated by RBF, the left picture shows the direct rendering of points (or particles for [7]) with estimated normal vectors. From the result of MST, it is easy to find that many points are displayed in black since their orientations are detected incorrectly. In the results of Cons [7] ((e)-(i)), h is a parameter for the support size of particles and $Iter$ stands for the number of iteration steps. The failure of Tight CoCone, ASC+Meshing and MST+RBF is mainly caused by the sparseness of input points. Producing a denser and more uniformly distributed set of points can improve the quality of reconstructed surfaces by them.

closest point search on M. The experimental results demonstrate that our approach can successfully orient the unorganized point clouds for various models – so that conventional schemes like [9] can reconstruct a proper surface for the input data. Figure 1 shows a comparison of the results between other approaches and ours on a Venus head model with non-uniform point density and noises. Our approach (ORT+RBF) gives the best reconstruction result. The good performance of our approach is benefited by 1) the proposed framework of using adaptive ASC to give the consistent orientation of points and 2) the newly developed sphere splitting step based on eigenvalue analysis.

2. RELATED WORK

The existing work in the literature can be classified into two major groups: 1) computational geometry approaches and 2) volumetric reconstruction techniques, which will be reviewed below.

The computational geometry approaches are usually based on the Voronoi diagram of a given point cloud and reconstruct a mesh surface by directly linking the input samples. Normal information is not required. Amenta et al. in [2] gave a provable guarantee of reconstructing

a correct model given a minimum sampling density dependent on the local feature size. The approach was further extended to be able to handle noisy input in [10]. However, as they did not remove outliers, the quality of the resultant meshes was not good. Several variations of [2] are available in [3], [4], [11], [12]. When applying these algorithms to practical data sets, there are two difficulties. First, both memory and time cost to compute Voronoi diagram are expensive. Second, such approaches request the input points to satisfy the d-covering requirement – i.e., the point set S sampled from the model H has any point $\mathbf{p}$ on H that can find a point $\mathbf{q} \in S$ such that $\|\mathbf{p} - \mathbf{q}\| \leq d$, where d is less than the smallest feature's size on M. This is hard to be satisfied, especially in the regions with highly sparse points and with noises embedded in S (see the examples shown in Fig.1 and Fig.16 where the Tight CoCone approach [4] fails). To the best of our knowledge, the integrating approach presented in [8] is a very good approach that can handle the above difficulties while does not need the input points to be equipped with normal vectors. However, their algorithm does not preserve the connectivity of underlying surfaces in the regions with very few points. Our extension of [8]

2

contributes to this.

The volumetric reconstruction techniques attempt to build a signed implicit function that interpolates or approximates the point cloud samples (ref. [1], [9], [13], [14], [15], [16], [17], [18]), and then extract its isosurface using, e.g., the Marching Cubes algorithm [19]. Nevertheless, the computation of such a signed implicit function requires the point cloud samples to be equipped with normal vectors, which can hardly be obtained directly from scanning devices. The estimation of consistently oriented normals on given cloudy points is actually one of the most critical steps in the reconstruction pipeline (ref. [1], [20]) – especially when the points are in the presence of noise, holes, sharp features, or thin structures. The most widely adopted approach to make the consistently oriented normal vectors is the orientation propagation algorithm using *minimal spanning tree* (MST) in [1], which however performs very poor on point clouds with the above defects. The orienting method presented in this paper overcomes these difficulties, and can generate consistently oriented normal vectors on unorganized points with noises, holes, sharp features and regions with highly sparse points. Moreover, compared with the conventional approach using MST, our method for orienting unorganized points is must faster.

The most recent work presented in [7] tries to address the similar problem as we do. However, their projection and down-sampling based strategy may destroy some small features of the underlying surface when the points are sparse. Our approach does not have such defect.

3. MODIFIED ADAPTIVE SPHERICAL COVER

The *adaptive spherical cover* (ASC) generated in [8] works well on a noisy point cloud $S = \{\mathbf{p}_1, \cdots, \mathbf{p}_n\}$ with n scattered points, and outputs a set of covering spheres which will be employed to construct triangular meshes by linking the auxiliary points in the spheres. To compensate the variation of point density on S, every point is assigned with a weight

$$w_i = \frac{1}{k} \sum_{j=1}^{k} \|\mathbf{p}_i - \mathbf{p}_j\|^2 \qquad (1)$$

where $\{\mathbf{p}_j\}_{j=1}^{k} \subset S$ are the k-nearest neighbors of $\mathbf{p}_i$. We select $k = 10$ in all our experimental tests, which well balances the speed and quality. Also, the unit normals $\{\mathbf{n}_1, \cdots, \mathbf{n}_n\}$ at the points of S are evaluated by their k-nearest neighbors using a standard covariance-based technique [1]. Note that, at this moment, the normal vectors are not necessary to be consistently oriented. Only their directions will be useful for the evaluation of quadric-error function below.

At the beginning of the spherical covering algorithm, all points in S are assigned as *uncovered*. Then, the algorithm will generate m spheres centered at $\{\mathbf{c}_1, \cdots, \mathbf{c}_m\} \subset S$ with the radii $\{r_1, \cdots, r_m\}$ chosen adaptively by repeating the following steps until no point is found to be uncovered.

1) Randomly select a point $\mathbf{c}_i$ from the set of uncovered points to serve as the center of a new sphere.
2) For each sphere, if its radius r was known, a quadric-error function centered at $\mathbf{c}_i$ is defined as

$$Q_{\mathbf{c}_i, r}(\mathbf{x}) = \sum_j w_j G_\sigma(\|\mathbf{p}_j - \mathbf{c}_j\|)(\mathbf{n}_j \cdot (\mathbf{x} - \mathbf{p}_j))^2$$
$$(2)$$

with $G_\sigma(\rho)$ being a compactly supported Gaussian-like function

$$G_\sigma(\rho) = \begin{cases} exp(-8(\rho/\sigma)^2), & |\rho| \in [0, \sigma/2] \\ 16(1 - \rho/\sigma)^4/e^2, & |\rho| \in (\sigma/2, \sigma] \\ 0. & |\rho| \in (\sigma, \infty] \end{cases}$$

The function $Q_{\mathbf{c}_i, r}(\mathbf{x})$ is locally defined on all the scattered points $\mathbf{p}_j$ falling in the range with $\|\mathbf{p}_j - \mathbf{c}_j\| \leq \sigma$. A practical choice for the support size is $\sigma = 2r$. The position $\mathbf{x}_{\min}$ which minimizes the value of $Q(\mathbf{c}_i, r, \mathbf{x})$ can be determined robustly through *singular value decomposition* (SVD) of the linear equations

$$\partial Q_{\mathbf{c}_i, r}(\mathbf{x})/\partial \mathbf{x} = 0.$$

The value of r is determined by solving the following nonlinear equation

$$Q_{\mathbf{c}_i, r}(\mathbf{x}_{\min}) = (\varepsilon L)^2, \qquad (3)$$

where L is the length of the main diagonal of the bounding box of point set S, and ε is an error control threshold ($\varepsilon = 10^{-5}$ is employed in all our tests).

3) After obtaining r, we check whether the point $\mathbf{x}_{\min}$ lies in the sphere $\|\mathbf{x} - \mathbf{c}_i\| \leq r$. If it does, $\mathbf{x}_{\min}$ serves as the auxiliary point of the sphere; otherwise, we simply assign the sphere center $\mathbf{c}_i$ as the auxiliary point.
4) Project the set of points in the sphere onto the tangent plane at $(\mathbf{x} - \mathbf{c}_i) \cdot \mathbf{c}_i = 0$, and then compute the 2D convex hull of the projections. The points not on the boundary of the 2D convex hull are labeled as covered.

The ASC generated by these steps will later be triangulated into mesh surfaces. Stimulated by the nerve complex associated with a family of balls [21], Ohtake et al. [8] created a triangle for every three spheres if and only if there exists two intersections points of them and at least one of the intersection points is *not* inside other spheres (except these three). The triangle links the auxiliary points in the spheres. Although non-manifold entities may be generated, they can be removed by the mesh cleaning step (details can be found in [8]). The mesh cleaning step will also propagate the consistent orientation along the resultant two-manifold mesh surface M.

The weights defined on points (Eq.(1)), which is based on the average distance to their k-nearest neighbors of $\mathbf{p}_i$, work according to the non-uniform density of the given points in some sense. However, such weights do
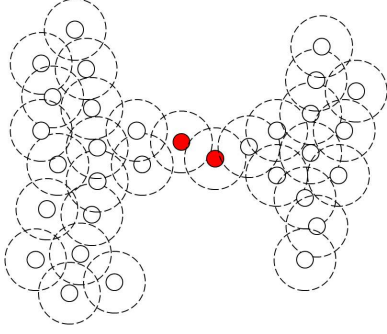
Fig. 2. Illustration of the problematic spheres generated by the ASC scheme [8] in anisotropic sparse regions – the red points and their corresponding spheres.

Fig. 4. Spheres in the anisotropic regions are detected (displayed in red) and split into sub-spheres.
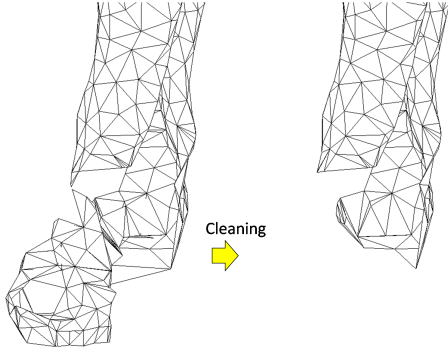

Fig. 3. The connectivity on separated regions is damaged in the cleaning step of [8] – the scattered points of this human body are shown in Fig.8.

not reflect the distribution of the points around a point $\mathbf{p}_i$. Based on this reason, the spheres generated by the above ASC scheme is problematic in the regions with very sparse points where the sparseness is *anisotropic*. An illustration of such a case is shown in Fig.2, where only one single line of spheres is constructed by the ASC scheme. As a result, no triangles (nor triangles linked by hanging vertices) can be generated around such spheres. Thus, the surfaces in the left and the right regions are separated on the resultant mesh M. The regions will be further separated after the cleaning step as the non-manifold entities will be removed. Figure 3 shows such a region on the feet of a human model from scanned raw data. The connectivity for linking these regions is important as breaking the connectivity may make two originally connected regions have opposite orientations – i.e., one is flipped. Such an orientation flip will fail the downstream surface reconstruction algorithm. To prevent the orientation flip, the best way is to avoid breaking the spheres connectivity of ASC in anisotropic sparse regions.

First, the spheres in the anisotropic sparse regions are detected. For a sphere $s_{\mathbf{c}_i}$ centered at $\mathbf{c}_i$, the spheres centered at $\mathbf{c}_j$ intersecting with $s_{\mathbf{c}_i}$ form its neighboring sphere set. Then, the neighbor voting tensor for the
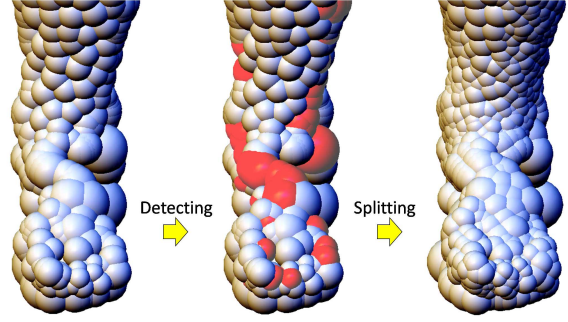
distribution of spheres around $s_{\mathbf{c}_i}$ is computed by

$$F_{\mathbf{c}_i} = \sum_j (\mathbf{c}_j - \mathbf{c}_i)(\mathbf{c}_j - \mathbf{c}_i)^T, \tag{4}$$

which is a 3×3 matrix. After computing the eigen-values ($|\lambda_1| \geq |\lambda_2| \geq |\lambda_3|$) of the neighbor voting tensor $F_{\mathbf{c}_i}$, if the other two eigen-values are trivial compared with the one with the greatest magnitude, the distribution of spheres around $s_{\mathbf{c}_i}$ should be anisotropic. In our practical implementation, we can detect spheres in the anisotropic distributed regions by checking if $|\lambda_1| > \mu|\lambda_2|$ with $\mu \in [2.0, 5.0]$. $\mu = 3.0$ is employed for all examples shown in this paper. Figure 4 shows the sphere detection on the foot example of Fig.3.

The spheres in the anisotropic sparse regions, which cannot preserve the connectivity of regions on their two sides during the triangulation and mesh cleaning, will be modified by a splitting scheme. Every such sphere is split into four sub-spheres. For a sphere $s_{\mathbf{c}_i}$ in the anisotropic region, its center $\mathbf{c}_i$ and the unit normal vector $\mathbf{n}_i$ at the center have been defined. If ν_1 is the eigen-vector of its neighbor voting tensor $F_{\mathbf{c}_i}$ corresponding to the largest eigen-value $|\lambda_1|$, we first project ν_1 onto the tangent plane $(\mathbf{x} - \mathbf{c}_i) \cdot \mathbf{n}_i = 0$ at $\mathbf{c}_i$.

$$\mathbf{v}_a = \frac{\nu_1 - (\nu_1 \cdot \mathbf{n}_i)\mathbf{n}_i}{\|\nu_1 - (\nu_1 \cdot \mathbf{n}_i)\mathbf{n}_i\|} \tag{5}$$

Its orthogonal vector on the tangent plane can then be found by the cross-product as $\mathbf{v}_b = \mathbf{n}_i \times \mathbf{v}_a$. The four sub-spheres split from $s_{\mathbf{c}_i}$ are located at

$$\mathbf{c}_i \pm \frac{r}{2}\mathbf{v}_a \pm \frac{r}{2}\mathbf{v}_b + \epsilon \tag{6}$$

with r being the radius of $s_{\mathbf{c}_i}$ and ϵ being a very small random perturbation for each sphere. $\frac{r}{2}$ is assigned as the radius of these sub-spheres. To enhance the robustness of this splitting scheme, we also split the spheres adjacent to (i.e., intersecting) the detected spheres in the anisotropic distributed regions. An illustration is given in Fig.5.

The points of the given point cloud covered by the sphere $s_{\mathbf{c}_i}$ will be checked to see if they are covered by the new sub-sphere. The auxiliary point in a new spheres is assigned by finding a point minimizing the quadratic-error function defined in Eq.(2). In addition, the new
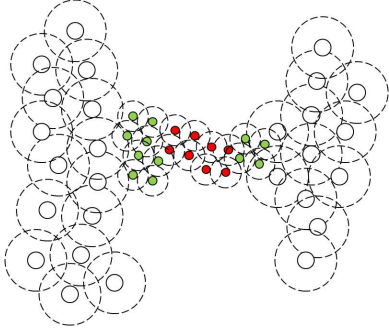
Fig. 5. Sphere splitting scheme: the red ones are split from the spheres in the anisotropic sparse regions, and the green ones are split from the neighboring spheres of the detected spheres.
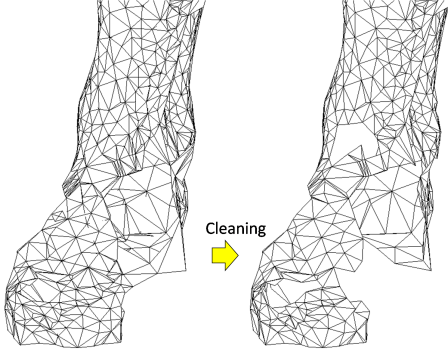

Fig. 6. The connectivity on separated regions is preserved after the cleaning step on the mesh generated from the modified adaptive spherical cover.
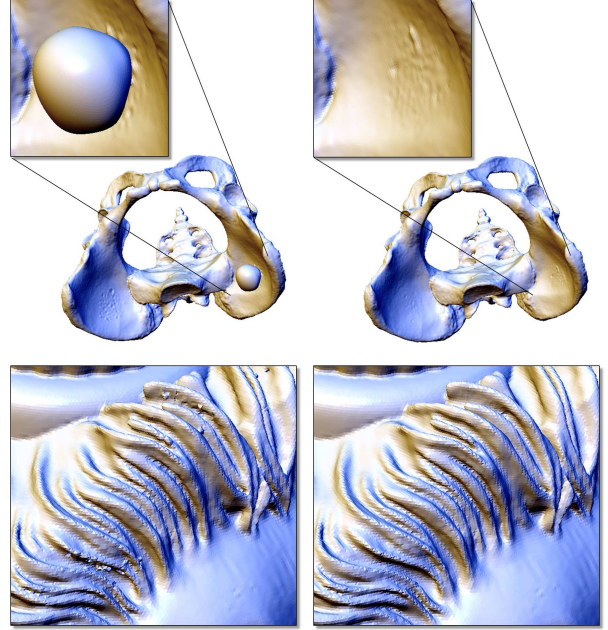

Fig. 7. The normal vectors estimated by the orientation-aware PCA scheme give better results than the direct transfer scheme and the direct flipping scheme on the reconstructed mesh surface using RBF approximation: (top-left) the reconstruction based on the normals from the direct flipping scheme, (top-right) from the orientation-aware PCA scheme, (bottom-left) the reconstruction by the normal from the direct transfer scheme, (bottom-right) result from the orientation-aware PCA scheme. The surfaces from the direct transfer scheme and the direct flipping scheme have some small separate spheres generated because of the errors on normal vectors of scattered points. The input points of the pelvis and the vase-lion models are given in Figs.10 and 11.

$\mathbf{x}_{\min}$ must be detected to see whether it is inside the corresponding sphere. If it is not, the sphere's center will simply be used as the auxiliary point. Note that, there is no guarantee that all the points originally covered by $s_{\mathbf{c}_i}$ will be covered by the new spheres. However, this will not affect the later meshing and normal estimation step of our algorithm. From the foot model example shown in Fig.6, we can easily find that the modified ASC scheme with sphere splitting step can better preserve the original shape on the underlying surface.

4. ORIENTING UNORGANIZED POINTS

After triangulating the auxiliary points in the modified adaptive spherical cover into a triangular mesh and cleaning its topology, we obtain a rough mesh surface M for approximating the underlying surface, which is represented by the input scattered data point S. Although M does not accurately approximate the shape of the underlying surface H, it gives a very good estimation of H's topology. Therefore, very good estimation of the orientation on H for the points in S can be found from M.

Basically, there are three ways to determine the normal vectors for the points of the given set $S = \{\mathbf{p}_1, \cdots, \mathbf{p}_n\}$. All need to first search the closest point $\mathbf{c}_{p_i}$ on the rough mesh surface M to every scattered point $\mathbf{p}_i$. The normal vector of $\mathbf{c}_{p_i}$ on M, $\mathbf{n}_{c_{p_i}}$, can also be obtained.

- *Direct Transfer:* Simply assign $\mathbf{n}_i = \mathbf{n}_{c_{p_i}}$.
- *Direct Flipping:* With the pre-computed unit normal vector $\mathbf{n}_i$ using PCA analysis, if $\mathbf{n}_{c_{p_i}} \cdot \mathbf{n}_i < 0$, let $\mathbf{n}_i = -\mathbf{n}_i$.
- *Orientation-aware PCA:* For the k neighboring points $\mathbf{p}_j$ around $\mathbf{p}_i$, only the points which satisfy $\mathbf{n}_{c_{p_j}} \cdot \mathbf{n}_{c_{p_i}} \geq 0$ are included to be applied with a new covariant *Principal Component Analysis* (PCA) to calculate a new normal vector $\mathbf{n}_i^{new}$ on $\mathbf{p}_i$.

The reconstructed mesh surface using the RBF based approach [9] is more sensitive to the orientation direction than the exact normal as the method does not really interpolate (or approximate) the normal vectors on the scattered points – instead, the off-points are generated to for approximating the inside/outside of the implicit surface. However, study still shows that the orientation-aware PCA scheme outperforms other two schemes in some examples (see Fig.7). Thus, the orientation-aware PCA scheme is adopted in our approach.

The only issue left unsolved now is how to efficiently find the closest point on M to the scattered point $\mathbf{p}_i$. A general solution for closest point search is to establish the *Bounding Volume Hierarchy* (BVH) (e.g., the *Swept Sphere Volume Hierarchy* (SSVH) presented in [22]). However, as the closest point search problem has its own characteristic, a faster approach can be developed

rather than using the general method like SSVH. This is because every vertex on the rough mesh M is always covered by spheres of the *adaptive spherical cover* (ASC). Moreover, most scattered points in S must also be covered by the spheres from ASC although there are very few escapees after the adaptive sphere splitting. Therefore, for a point $\mathbf{p}_i$ from S, if it is covered by a sphere ϱ, its closest point will be searched on the triangles of a set T_{set}. T_{set} includes all the triangles with at least one vertex enclosed by ϱ. If the vertex enclosed by ϱ has been removed during the mesh cleaning process, the triangles adjacent to the vertices enclosed by ϱ_{neigh} will be included into T_{set}. Here, ϱ_{neigh} are spheres intersecting ϱ. If the point $\mathbf{p}_i$ is not covered by any sphere, we will select the sphere who covers the closest neighbor of $\mathbf{p}_i$ as ϱ to determine the set T_{set} of triangles. In the experimental tests shown in the section below, we compare the search conducted by SSVH with this local search scheme. The results show that ours is three to four times faster than SSVH as the construction of SSVH takes a lot of time while ours only use the ASC structure which has already been established.

5. RESULTS

The proposed approach has been implemented in Visual C++. Our implementation has been tested on a variety of models. The statistics in this paper are all tested on a standard PC with Intel Core 2 CPU 6600 at 2.4GHz plus 2.0GB RAM.

The first example tested is the Venus head model with noises and non-uniform sparseness, which is shown in Fig.1. Note that making the density of points much farther sparse may lead our method also failed, so as others. Our method gives better result than other approaches here. The second example is the real data of a human model captured by a laser-based human scan system with only two column laser scanners. Note that different from the previous system with four or six columns, the points are roughly two pieces – one is captured from the front and another from the back (see Fig.8). The reconstructions from the Tight CoCone [4] and the integrating approach (ASC + Meshing) [8] do not give a good surface approximation at the place where no scan point is presented. The conventional normal orienting method (MST) [1] will generate flipped orientation on the front and back parts of a human model, so the resultant implicit surface from RBF based reconstruction [9] will have wrong topology. The surface generated from the down-sampled particles and their normals from the consolidation scheme (Cons) [7] give a very poor shape to the right foot of the human body. This is because the points are highly sparse in that region, and the down-sampling strategy from [7] further damages the very limited number of data points there. Similar effects from the consolidation approach can also be found in other examples shown below. The parameter h used in all the tests here are chosen by a trial and
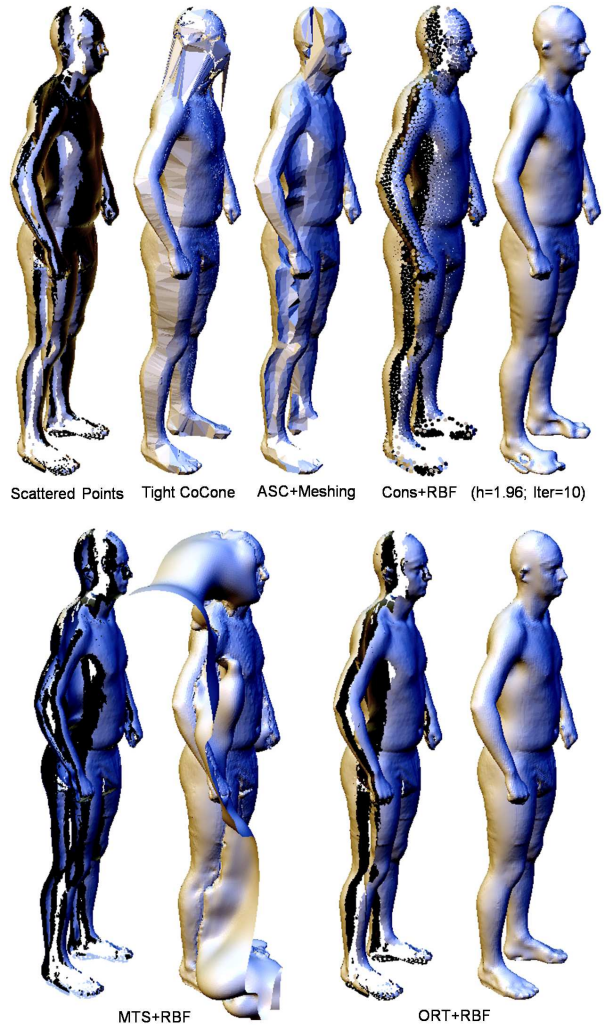

Fig. 8. Surface reconstruction results on a human model with 170k points by different approaches.

error procedure – we try several values for h, the one with best reconstruction result is displayed. Furthermore, when testing the consolidation approach [7], in order to estimate the normals correctly we apply the normal propagation and the orientation-aware PCA iteratively for five to ten times in all tests. Another example for the reconstruction of human body is shown in Fig.9. The fourth example is to test our method on a pelvis model with a more complex topology (i.e., with high genus number). From the results shown in Fig.10, it is easy to find that other approaches are likely to produce an incorrect topology on the resultant surfaces because of incorrect orientations assigned to sample points.

The following examples are conducted to test the performance of our approach versus others on models with sharp (or thin) features. The first try is given on a vase-lion model with 182k points (see Fig.11) – there are many small and thin features on the lion's hair. The conventional *minimal spanning tree* (MST) based normal propagation followed by a RBF-based surface reconstruction will destroy some of the small features as incorrect normal orientations are assigned to some
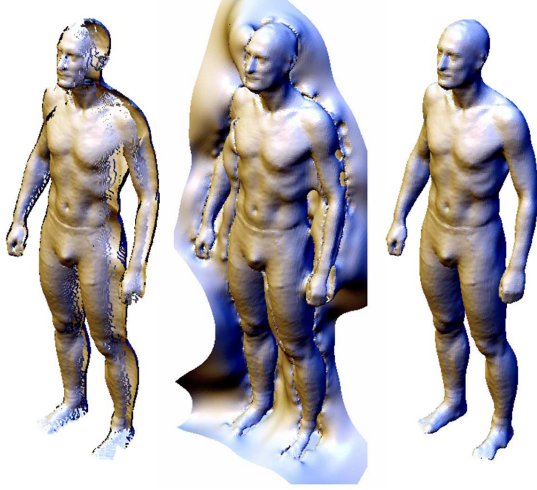
Fig. 9. Surface reconstruction results on another human model with 85.8k points: (left) the given scattered points, (middle) the reconstruction by MST+RBF, and (right) the reconstructed result by our method.
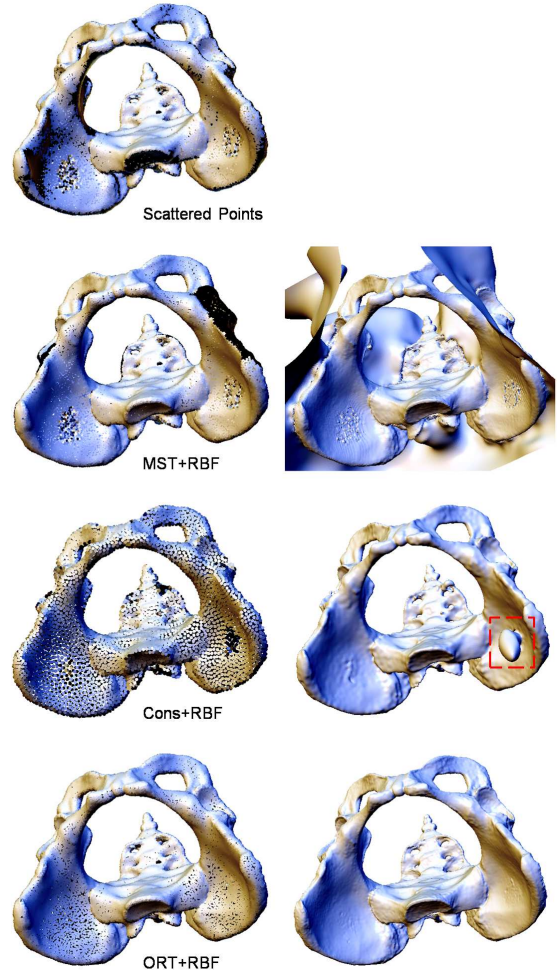

Fig. 10. Surface reconstruction results on the pelvis model (50.7k points) by different approaches. Left column displays the points with oriented normal vectors – incorrect normal may disable some points from being displayed. The MST+RBF approach generates a surface with an incorrect topology, and the Cons+RBF (with $h = 13.8$, $\mu = 0.45$ and $Iter = 50$) produces an extra enclosure which is not suggested by the input data (circled by the red dash line). All these are led by the incorrectly oriented normals generated by their approaches.

points – see the points displayed in black in Fig.11. When testing this vase-lion model on the executable program shared by the authors of [7], the program surprisedly crashed in the normal propagation step. Our normal orienting approach can successfully assign correct orientations to the given points so that a correct vase-lion model can be reconstructed. The second example of the reconstruction with thin features is a blade model (see Fig.12). The thin feature is also damaged by the consolidation approach [7] as the point density on the given point cloud is not high enough to make the thin feature survive during down-sampling. Even if working on the dense point cloud, our method still does outperform other approaches – see the last example of a scissor model with sharp features in Fig.13. Again, the MST+RBF approach cannot reconstruct surface with a correct topology, and the Cons+RBF method gives a bad shape at the tip. To further evaluate the oriented normal vectors constructed by our approach, we apply them to another volumetric reconstruction approach – Poisson surface reconstruction [18]. Comparison of results for the scissor model using oriented normals generated by different approaches can be found in Fig.14. Moreover, points equipped with the oriented normal vectors generated by our approach have the capability to present complex geometry details on the reconstructed surfaces (see the example shown in Fig.15).

Another interesting study is about the efficiency of our algorithm presented in this paper compared with the minimal spanning tree based conventional approach and the recently presented consolidation approach in [7]. In fact, the speed of our local search based scheme compared with the global method using SSVH [22] is also given. The computational statistics are shown in Table 1. From them, it is easy to find that our orienting approach is much faster than the conventional approach using minimal spanning tree on those large models. Ours

is also more efficient than the consolidation approach. Benefited by the already constructed ASC structure, the local search based normal orienting is about three to four times faster than the global search using SSVH.

A major limitation of our approach is that we will also process the outliers in the given points as we do not modify the points (e.g., the incomplete model shown in Fig.16 with outliers and structured noises). However, after checking all other approaches, it seems none approach can generate satisfactory results when using RBF-based surface reconstruction. When applying the Poisson surface reconstruction approach, only the oriented normal vectors generated by our approach (ORT) can give satisfactory result (see the bottom row of Fig.16).

TABLE 1
COMPUTATIONAL STATISTICS

| Model | Figure | Points Num. | Time of MST (sec.) | Consolidation | | Time of Our Approach (sec.) | | Time of SSVH |
				Particles Num.	Time† (sec.)	Modified ASC	Local Search	
Venus	1	72.5k	38.5	7,255	36.9 + 7.0	4.6	0.6	2.4
Human-body I	8	170k	93.0	8,518	23.1 + 10.0	4.7	0.7	2.2
Human-body II	9	85.8k	24.8	17,151	32.7 + 32.0	2.6	0.3	1.2
Pelvis	10	50.7k	17.7	10,137	13.0 + 17.0	3.3	0.4	1.3
Vase-lion	11	182k	166.4	Failed*	Failed*	6.0	0.7	4.3
Blade	12	25k	3.7	5,000	6.8 + 5.5	1.5	0.2	0.6
Scissor	13	212k	248.6	10,616	34.7 + 14.0	10.0	1.0	3.5
Fish	15	217k	247.5	21,698	44.6 + 19.3	5.2	0.6	2.6
Filigree	15	250k	330.3	25,000	39.4 + 50.5	13.8	1.6	4.5

†The time for the consolidation approach has two components: weighted LOP (former) and normal estimation (latter).
*The test of vase-lion model is failed in the executable program provided by the authors of the consolidation approach [7].
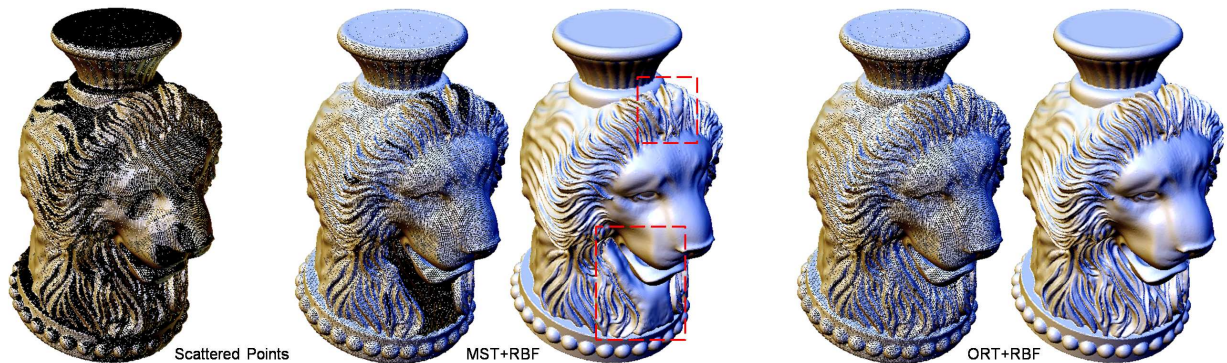

Fig. 11. Surface reconstruction results on the vase-lion model (182k points) by MST+RBF versus ORT+RBF. Many small features are damaged by the MTS+RBF approach (circled by red dash lines).

6. CONCLUSION AND DISCUSSION

In this paper, we have presented a robust and efficient method to assign consistently oriented normal vectors to unorganized points with noises, non-uniformities, and thin sharp features as a pre-processing step to surface reconstruction. The conventional method for this normal assignment step is through the minimal spanning tree based normal propagation, which however is not robust on the unorganized points with noises, non-uniformities, and thin sharp features. The newly developed point consolidation approach [7] tries to overcome such difficulties. Different from [7], our approach does not modify (i.e., down-sample) the given point cloud so that it can reconstruct more surface details than the consolidation approach in the regions with very few points. Our orienting approach consists of three steps: 1) modified ASC generation, 2) meshing and cleaning, and 3) local search based normal orienting. Experimental results prove that our approach can successfully orient the unorganized point clouds for various models, which benefits the downstream surface reconstructions.

A possible future work is to process the points by the robust statistics based method presented in a recent work (ref. [23]). Of course, this does not agree with the spirit of our approach as the points are modified, which may also destroy the geometry details on the underlying surfaces. To solve this problem will be one
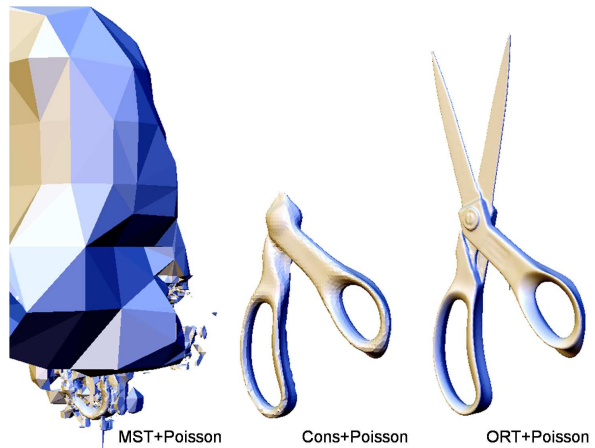

Fig. 14. Surface reconstruction results on the scissor model (212k points) by Poisson surface reconstruction [18] using different approaches to generate oriented normal vectors.

of our major future work. Another challenging problem is how to handle the structural noises, which will also be considered in our future work.
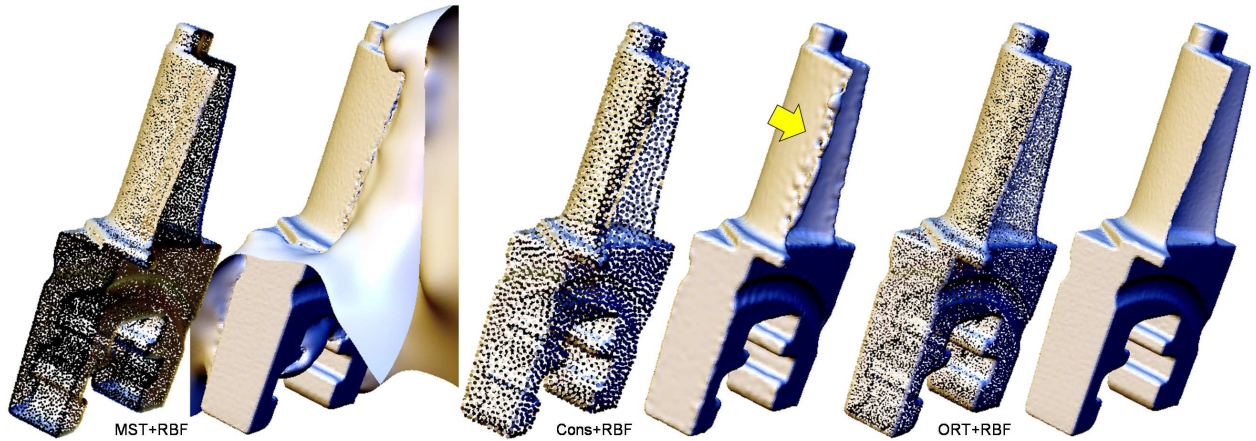
Fig. 12. Surface reconstruction results on the blade model (25k points) by different approaches. A surface with an incorrect topology is output by the MST+RBF approach, and thin features (pointed by yellow arrow) are damaged by the Cons+RBF approach (with $h = 3.99$, $\mu = 0.45$ and $Iter = 50$).
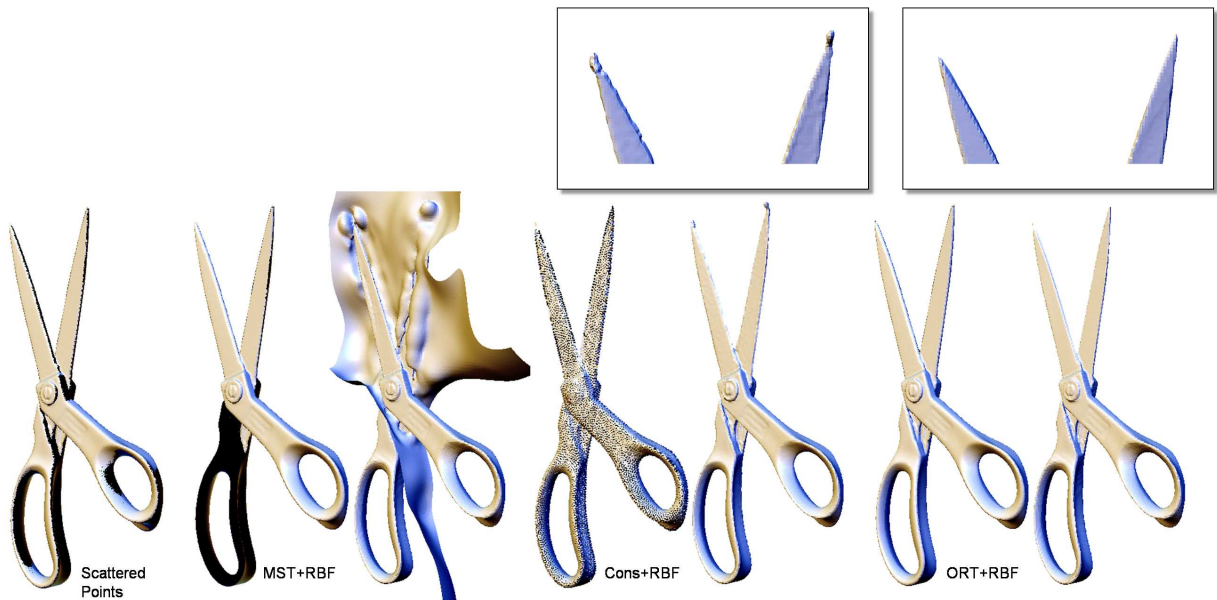

Fig. 13. Surface reconstruction results on the scissor model (212k points) by different approaches. A surface with an incorrect topology is output by the MST+RBF approach, and sharp features at the tip of the scissor are damaged by the Cons+RBF approach (with $h = 2.07$, $\mu = 0.45$ and $Iter = 50$).

REFERENCES

[1] H. Hoppe, T. DeRose, T. Duchamp, J. McDonald, and W. Stuetzle, "Surface reconstruction from unorganized points", *In Proceedings of ACM SIGGRAPH 1992*, pp.71-78, 1992.

[2] N. Amenta, M. Bern, and M. Kamvysselis, "A new voronoi-based surface reconstruction algorithm", *In Proceedings of ACM SIGGRAPH 1998*, pp.415-421, 1998.

[3] N. Amenta, S. Choi, and R. Kolluri, "The power crust", *In Proceedings of 6th ACM Symposium on Solid Modeling*, pp.249-260, 2001.

[4] T.K. Dey, and S. Goswami, "Tight cocone: A watertight surface reconstructor", *In Proc. 8th ACM Sympos. Solid Modeling Applications*, pp.127-134, 2003.

[5] J. Sun, M. Smith, L. Smith, and A. Farooq, "Examining the uncertainty of the recovered surface normal in three light photometric stereo", *Image and Vision Computing*, vol.25, no.7, pp.1073-1079, 2007.

[6] W.-C. Ma, T. Hawkins, P. Peers, C.-F. Chabert, M. Weiss, and P. Debevec, "Rapid acquisition of specular and diffuse normal maps from polarized spherical gradient illumination", *In Eurographics Symposium on Rendering*, pp.183-194, 2007.

[7] H. Huang, D. Li, H. Zhang, U. Ascher, and D. Cohen-Or, "Consolidation of unorganized point clouds for surface reconstruction", *In Proc. of SIG-
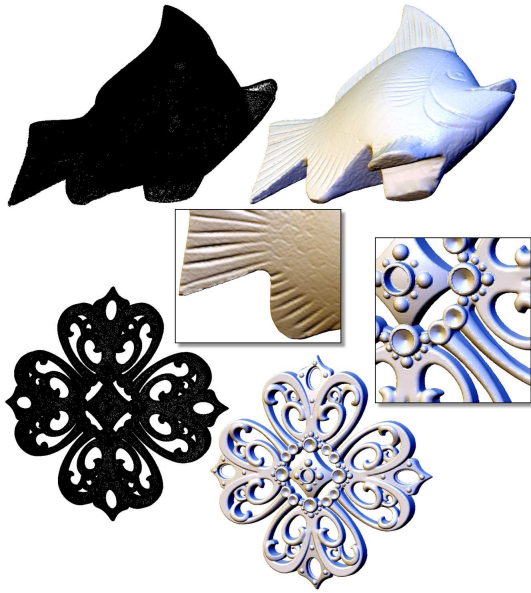
Fig. 15. Surface reconstruction results on the fish model (217k points) and the filigree model (250k points) by our orienting approach plus the RBF based reconstruction.

Scattered Points   Tight CoCone   ASC+Meshing

MST+RBF   Cons+RBF   ORT+RBF

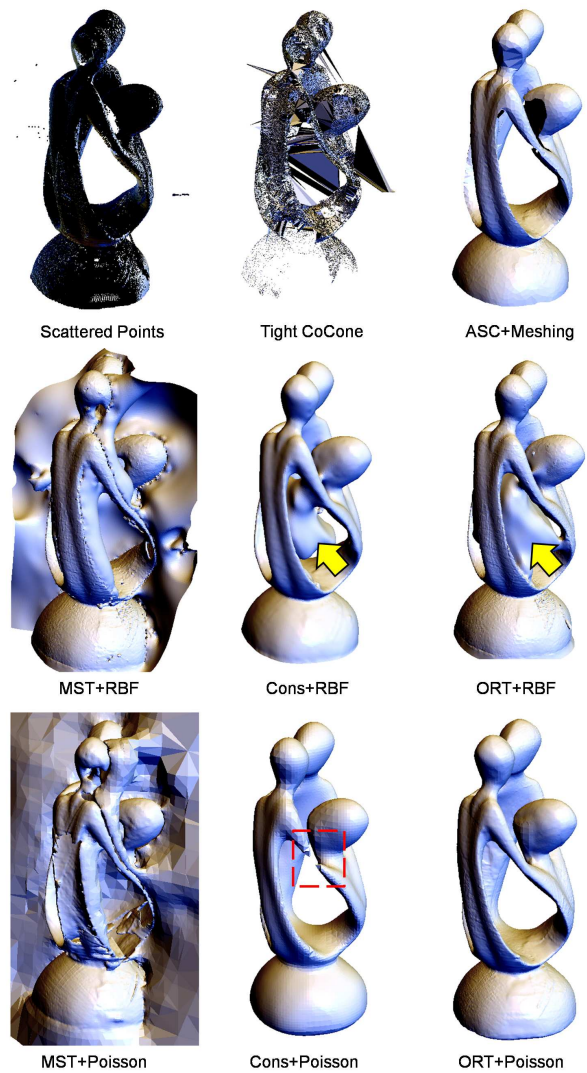MST+Poisson   Cons+Poisson   ORT+Poisson

Fig. 16. Surface reconstruction results on the incomplete scattered data of a model with outliers and structured noises. None approach can generate satisfactory result. Top row – input scattered points and surface reconstructed by the computational geometry approaches; middle row – the surfaces are reconstructed using RBF-based reconstruction where unreasonable surface parts (pointed by the yellow arrow) are generated on the resultant surfaces by Cons+RBF [7] and our ORT+RBF; bottom row – the surfaces are generated by Poisson surface reconstruction [18] where only ours is satisfactory.

GRAPH Asia 2009, 2009.

[8] Y. Ohtake, A. Belyaev, and H.-P. Seidel, "An integrating approach to meshing scattered point data", *In Proc. of ACM Symposium on Solid and Physical Modeling (SPM 2005)*, pp.61-69, 2005.

[9] Y. Ohtake, A. Belyaev, and H.-P. Seidel, "3D scattered data interpolation and approximation with multilevel compactly supported RBFs", *Graphical Models*, vol.67, no.3, pp.150-165, 2005.

[10] B. Mederos, N. Amenta, L. Velho, and L. H. de Figueiredo, "Surface reconstruction from noisy point clouds", *In SGP 05: Proceedings of the third Eurographics symposium on Geometry processing*, pp.53, 2005.

[11] T.K. Dey, J. Giesen, and J. Hudson, "Delaunay based shape reconstruction from large data", *In Proc. of the IEEE 2001 symposium on parallel and large-data visualization and graphics*, pp.19-27, 2001.

[12] C.-C. Kuo, and H.-T. Yau, "A new combinatorial approach to surface reconstruction with sharp features", *IEEE Transactions on Visualization and Computer Graphics*, vol.12, no.1, pp.73-82, 2006.

[13] J.C. Carr, R.K. Beatson, J.B. Cherrie, T.J. Mitchell, W.R. Fright, B.C. McCallum, and T.R. Evans, "Reconstruction and representation of 3D objects with radial basis functions", *In Proceedings of SIGGRAPH '01*, pp.67-76, 2001.

[14] G. Turk, and J.F. O'Brien, "Modelling with Implicit Surfaces that Interpolate", *ACM Transactions on Graphics*, vol.21, no.4, pp.855-873, 2002.

[15] H.Q. Dinh, G. Turk, and G. Slabaugh, "Reconstructing surfaces by volumetric regularization using radial basis functions", *IEEE Transactions on Pattern Analysis and Machine Intelligence*, vol.24, no.10, pp.1358-1371, 2002.

[16] G. Yngve, and G. Turk, "Robust creation of implicit surfaces from polygonal meshes", *IEEE Transactions on Vizualization and Computer Graphics*, vol.8, no.4, pp.346-359, 2002.

[17] Y. Ohtake, A. Belyaev, M. Alexa, G. Turk, and P.-H. Seidel, "Multi-level partition of unity implicits", *ACM Transactions on Graphics*, vol.22, no.3, pp.463-470, 2003.

[18] M. Kazhdan, M. Bolitho, and H. Hoppe, "Poisson surface reconstruction", *In Proc. of Eurographics Symposium on Geometry Processing 2006*, pp.61-70, 2006.

[19] W.E. Lorensen, and H.E. Cline, "Marching cubes: A high resolution 3d surface construction algorithm", *SIGGRAPH Computer Graphics*, vol.21, no.4, pp.163-169, 1987.

[20] V. Mello, L. Velho, and G. Taubin, "Estimating the in/out function of a surface represented by points", *In Proceedings of the Eighth ACM Symposium on Solid Modeling and Applications*, pp.108-114, June 16-20, 2003.

[21] J. Rotman, *An Introduction to Algebraic Geometry*, 1988, Springer.

[22] E. Larsen, S. Gottschalk, M.C. Lin, and D.

Manocha, "Fast proximity queries with swept sphere volumes", *Proc. of International Conference on Robotics and Automation*, pp.3719-3726, April 2000.

[23] H. Sheung, and C.C.L. Wang, "Robust mesh reconstruction from unoriented noisy points", *Proc. of ACM Symposium on Solid and Physical Modeling 2009*, pp.13-24, San Francisco, California, October 5-8, 2009.